Band-Mott mixing hybridizes the gap in $Fe_2Mo_3O_8$

K. Park,[1] G. L. Pascut,[2, 3] G. Khanal,[3] M. O. Yokosuk,[1] Xianghan Xu,[3] Bin Gao,[4] M. J. Gutmann,[5] A. P. Litvinchuk,[6] V. Kiryukhin,[3, 7] S. -W. Cheong,[3, 7, 8] D. Vanderbilt,[3] K. Haule,[3] and J. L. Musfeldt[1, 9, *]

[1]*Department of Chemistry, University of Tennessee, Knoxville, Tennessee 37996, USA*
[2]*MANSiD Research Center and Faculty of Forestry, Applied Ecology Laboratory,*
Stefan Cel Mare University (USV), 13 University Rd, Suceava 720229, Romania
[3]*Department of Physics and Astronomy, Rutgers University, Piscataway, New Jersey 08854, USA*
[4]*Department of Physics and Astronomy, Rice University, Houston, Texas 77005, USA*
[5]*ISIS Facility, STFC-Rutherford Appleton Laboratory, Didcot OX11 OQX, United Kingdom*
[6]*Texas Center for Superconductivity and Department of Physics,*
University of Houston, Houston, Texas 77204, USA
[7]*Rutgers Center for Emergent Materials, Rutgers University, Piscataway, New Jersey 08854, USA*
[8]*Laboratory for Pohang Emergent Materials and Max Planck POSTECH Center for Complex Phase Materials,*
Pohang University of Science and Technology, Pohang 790-784, Korea
[9]*Department of Physics and Astronomy, University of Tennessee, Knoxville, Tennessee 37996, USA*

(Dated: November 5, 2020)

We combine optical spectroscopy and first principles electronic structure calculations to reveal the microscopic character of the charge gap in the polar magnet $Fe_2Mo_3O_8$. Iron occupation on the octahedral site draws the gap strongly downward compared to the Zn parent compound, whereas occupation on the tetrahedral site creates a narrow resonance near the Fermi energy that emanates from a flat valence band in a Mott-like state due to screening of the local moment - similar to expectations for a Zhang-Rice singlet. We discuss this unusual hybridization in terms of orbital occupation and character as well as the structure-property relationships that can be unveiled in various metal-substituted systems (Ni, Mn, Co, Zn).

INTRODUCTION

While 3*d*-containing materials are well known for strong electron correlations, narrow band widths, site- and orbital-selective states, and robust magnetism, 4*d* and 5*d* systems are recognized for strong spin–orbit coupling, increased hybridization, extended orbitals, and a tendency toward dimerization [1]. Combining these traits in mixed metal materials leads to variety of unexpected properties. Examples include interpenetrating sublattices with independent spin dynamics and ground states in Sr_2CoOsO_6 [2, 3], self-healing photoelectrode materials like $CuRhO_2$ [4], covalency-driven collapse of spin-orbit coupling in $Ba_5CuIr_3O_{12}$ [5], an ultra-high coercive field in Sr_3NiIrO_6 [6, 7], magnetoelectric coupling in $Co_4Nb_2O_9$ [8], surprising spin entropy effects across the magnetic quantum phase transition in $CoNb_2O_6$ [9], and nonreciprocal directional dichroism in Ni_3TeO_6 [10]. Another mixed metal system with exciting properties and curious hybridization is $Fe_2Mo_3O_8$ - also known as the mineral Kamiokite [11]. While magnetism and magnetoelectric coupling have been widely studied [12–19], the charge excitations are highly under-explored.

$Fe_2Mo_3O_8$ is a polar magnet with giant magnetoelectric coupling, strong Dzyaloshinski-Moriya interactions, valence bond condensation (creating a cluster magnet), and the possibility of orbitally-selective transitions [12–19]. Zinc substitution, first on the tetrahedral Fe site and then on the octahedral Fe site [15, 20], is of interest for magnetic properties as well [11, 13, 20, 21]. The structure of $Fe_2Mo_3O_8$ consists of corner-shared tetrahedral and octahedral sites separated by layers of Mo trimers [Fig. 1(a,b)] [12, 22, 23]. This system has a 61 K magnetic ordering transition to a collinear antiferromagnetic state with a concomitant structural distortion [14, 24–27]. Antiferromagnetic antiphase domain boundaries have been imaged in this state [28]. There is also a 5 T transition to the ferrimagnetic state, with an extremely large magnetoelectric coefficient [14, 15]. Spectroscopic highlights include (i) nonreciprocal directional dichroism [29], phonon trends across T_N [26, 27], and a variety of magnetic excitations in the terahertz range [30], (ii) Mössbauer to confirm the 2+ charge on the iron site [24, 25], and (iii) studies of charge transfer via time-dependent optical Kerr effects [31] complemented by first principles electronic structure calculations [20, 27, 32].

In order to place the charge excitations on a firm foundation, we measured the optical properties of $A_2Mo_3O_8$ (where A = Fe, Ni, Mn, Zn) and compared our findings with complementary electronic structure calculations. We show that the 1.7 eV gap in $Zn_2Mo_3O_8$ is determined by the charge excitations of the Mo trimer. Replacing Zn on the octahedral site with Fe yields $FeZnMo_3O_8$. This system has a substantially reduced and renormalized gap determined by Fe-O hybridized bands that appear due to the periodic lattice potential. In contrast, $Fe_2Mo_3O_8$ has both octahedral and tetrahedral sites occupied by Fe atoms, and the gap is further reduced to 1.0 eV. In this case, the charge gap is more complex to describe and has mixed band and Mott features, namely, some orbitals hybridize strongly with oxygen and form very narrow bands, while other orbitals exhibit real space localiza-

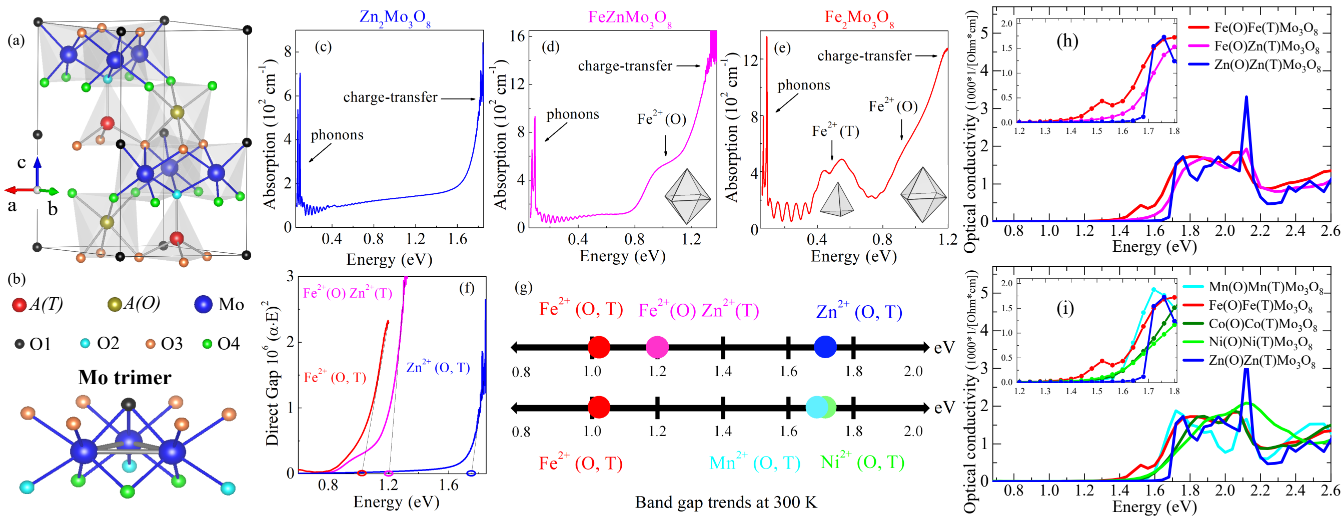

FIG. 1. (a) Crystal structure of the $A_2Mo_3O_8$ compounds, where A = Mn, Fe, Co, Mn, Zn. A(T) and A(O) represent ions inside the tetrahedra and octahedral environments, respectively. (b) Schematic view of the Mo trimmer. (c-e) Absorption spectra of $Zn_2Mo_3O_8$, $FeZnMo_3O_8$, and $Fe_2Mo_3O_8$ at room temperature. (f) A Tauc plot reveals the direct band gap of $Fe_2Mo_3O_8$ and the Zn-substituted analogs. (g) Band gap schematic showing the impact of two different types of T and O-site substitution. The upper and lower trend lines correspond to the $(Fe,Zn)_2Mo_3O_8$ series and the $A_2Mo_3O_8$ (A = Fe, Mn, Ni) materials, respectively. (h,i) Calculated ptical conductivity for the $A_2Mo_3O_8$ materials.

tion and are Mott insulating. Mixed band- or metal-Mott gaps are commonly called orbitally- or site- selective Mott states [33–38]. What distinguishes $Fe_2Mo_3O_8$ from other orbitally-selective Mott systems is the narrow resonance emanating from the flat valence band. The latter has strong many-body character. The gap in $Fe_2Mo_3O_8$ is sensitive to magnetic ordering at 61 K due to the heavily mixed character of the charge excitations. Moreover, the d-to-d excitations on the octahedral Fe site are vibronically activated, and spin-orbit related features ride on top of the tetrahedral on-site excitations below the magnetic ordering transition. We discuss these findings in terms of band-Mott mixing in $3d^6$- and $4d$-containing quantum cluster magnets.

METHODS

High quality single crystals of $Fe_2Mo_3O_8$, the Zn-substituted analogs $FeZnMo_3O_8$, and $Zn_2Mo_3O_8$, as well as $Mn_2Mo_3O_8$ and $Ni_2Mo_3O_8$ were grown by chemical vapor transport as discussed previously [14]. Crystals were polished to control optical density and expose the hexagonal face. A Bruker 55 Fourier transform infrared spectrometer equipped with a microscope attachment was used to measure transmittance over the 0.41 - 2.0 eV energy range. Absorption was calculated as $\alpha(E) = -\frac{1}{d}\ln(\mathcal{T}(E))$, where $\mathcal{T}(E)$ is the transmittance and d is the thickness. Temperature was controlled by an open-flow cryostat.

For theoretical calculations we used the density functional theory (DFT) as implemented in WIEN2k [39] and a charge-self-consistent dynamical mean field theory (DMFT) as implemented in the eDMFT code [40–44]. At the DFT level, we used the generalized gradient approximation Perdew-Burke-Ernzerhof (GGA-PBE) functional [45], with RKmax = 7.0 and 1026 k-points in the irreducible part of the 1st Brillouin zone. At the eDMFT level, we used the fully rotationally invariant Coulomb interaction, a nominal double counting scheme [46], with the d-orbital occupations for double counting corrections for Mn, Fe, Co and Ni set to be 5, 6, 7 and 8, respectively. To define the DMFT projector, we used the quasiatomic orbitals by projecting bands in a large hybridization window (-10 to +10 eV) with respect to the Fermi level, in which partially screened Coulomb interaction has values of U = 10 eV and J_H = 1 eV in Mn, Fe, Co and Ni ions. In order to solve the auxiliary quantum impurity problem, a continuous-time quantum Monte Carlo method in the hybridization-expansion (CT-HYB) was used [47], where the five d orbitals for the Mn, Fe, Co and Ni ions (grouped according to the local C_{3v} point group symmetry) were chosen as our correlated subspace in a single-site DMFT approximation. For the CT-HYB calculations, up to 2 $\times$ 10^8 Monte Carlo steps were employed for each Monte Carlo run. The experimental crystal structures used for our theoretical calculations [26] are given in the Supplementary information.

RESULTS AND DISCUSSION

Optical response of $Fe_2Mo_3O_8$ and the A-substituted analogs (A = Zn, Mn, Ni)

Figure 1(c-e) summarizes the optical properties of the (Fe,Zn)Mo_3O_8 family of materials. The absorption spectrum of the parent compound, $Zn_2Mo_3O_8$, is low and flat in the near infrared, rising on approach to the O 2*p* → Mo 3*d* charge transfer excitation. The experimental direct band gap is at 1.75 eV. Because Zn^{2+} is in the d^{10} configuration, there are no *d*-to-*d* on-site excitations. $Zn_2Mo_3O_8$ therefore provides an opportunity to study how the Mo trimer interacts with oxygen in isolation. At the same time, it is an important scaffold upon which additional complexity can be built.

Sequential *A*-site substitution of Fe, first into the octahedral site in $FeZnMo_3O_8$, here denoted as Fe(O), and then into the tetrahedral site in $Fe_2Mo_3O_8$, henceforth Fe(T), lowers the charge gap significantly [Fig. 1(f)]. We find direct gaps of 1.2 and 1.0 eV for $FeZnMo_3O_8$ and $Fe_2Mo_3O_8$, respectively. The gap values were determined from Tauc plots [48] of $(\alpha{\cdot}E)^2$ vs. energy.

Figure 1(d) displays the absorption of $FeZnMo_3O_8$. The charge excitations across the gap consist of mixed O 2*p* + Mo 3*d* + Fe(O) 3*d* transitions. The lowest energy excitation across this gap comes from Fe(O) hybridizing with Mo-O trimers. The 1.2 eV gap is substantially lower in energy than the fundamental Mo-O band gap, which theoretically remains roughly equal to that in $Zn_2Mo_3O_8$. As Fe^{2+} populates the octahedral site in $FeZnMo_3O_8$, an on-site *d*-to-*d* transition arises near 0.95 eV. It strongly overlaps with the leading edge of the charge transfer band. Once the Fe(T) site is populated as well (as in $Fe_2Mo_3O_8$), the gap is reduced further, and two different types of *d*-to-*d* on-site excitations are identified inside the charge gap. As shown in Fig. 1(e), the tetrahedral site contributes additional atomic-like excitations centered at 0.5 eV. These *d*-to-*d* in-gap excitations are further discussed in the Supplementary information. The full sequence of band gaps is summarized in Fig. 1(g).

To test the influence of *A*-site substitution on the band gap and strength of the metal to MoO-trimer hybridization, we measured the optical properties of the Mn and Ni analogs of $Fe_2Mo_3O_8$ [Fig. S1, Supplementary information]. $Mn_2Mo_3O_8$ and $Ni_2Mo_3O_8$ have charge gaps of 1.65 and 1.7 eV, respectively - very similar to that of the Zn end member. This result is attributable to the 3*d* orbital filling and character. The Mn system has a half-filled *d*-manifold, which corresponds to a high spin Mott state with a large gap. The d^8 configuration in the Ni compound also has two holes and is thus in the large gap Mott insulating state. As a result, there is little mixing between the metal center and Mo-O trimer, hence these transition metals do not play an active role in determining the low-energy excitations across the gap. We mention in passing that both the Mn and Ni compounds also have on-site *d*-to-*d* excitations [Fig. S1, Supplementary information].

On the other hand, $Fe_2Mo_3O_8$ has both Mott-type and band-insulating orbitals, which strongly hybridize with the Mo trimer. This interaction activates the Fe centers to play an important role in the low energy physics as discussed below. As a consequence, the band gap is sensitive to the 61 K magnetic ordering transition and its associated structural distortion [Fig. S10(a,d), Supplementary information]. This is different from the other $A_2Mo_3O_8$ compounds, where the temperature dependence of the band gaps are in excellent overall agreement with the Varshni model [49, 50] implying no (or extremely subtle) structural transitions. That the band gap decreases across T_N is due to charge-lattice-spin coupling and the flat bands emanating from the quasi-tetrahedral Fe site.

Strong hybridization, resonance, and interaction with the Mo trimer

Figure 1(h) shows the theoretical optical conductivity of $Zn_2Mo_3O_8$, $FeZnMo_3O_8$ and $Fe_2Mo_3O_8$ computed using a combination of Density Functional Theory and embedded Dynamical Mean Field Theory (DFT + eDFMT) methods [40–44]. Here, we find the same trend of decreasing theoretical charge gap with Fe substitution. In $Zn_2Mo_3O_8$, the optical gap size is ≈1.7 eV which decreases to around 1.5 and 1.4 eV in $FeZnMo_3O_8$ and $Fe_2Mo_3O_8$, respectively. Figure 1(i) compares the predicted optical conductivity of the Mn, Ni and Co analogs. We find that the predicted gap is larger in all of these compounds (around 1.55 eV) as compared to $Fe_2Mo_3O_8$, and the edge of the gap is very smooth and temperature smeared. This is quite different from that of $Fe_2Mo_3O_8$, where the gap is smaller and has an additional peak at the onset.

To better understand what determines the low-energy excitations and the character of the gap in this class of compounds, we calculated the local density of states for the $A_2Mo_3O_8$ compounds [Fig. 2]. While the optical gap in general is different than the gap of the single-particle excitations measured by the local density of states, in these compounds the two are very similar. This is because the band gap is direct in $Zn_2Mo_3O_8$, and the hybridized bands in the Fe compounds are extremely narrow, hence momentum conserving excitations have essentially the same gap size as the finite momentum single particle excitations. The insets show that the conduction band in $FeZnMo_3O_8$ and $Fe_2Mo_3O_8$ slightly decreases as compared to $Zn_2Mo_3O_8$, but the change is small. Most of the action is in the valence bands, where the FeZn band edge moves considerably upward, and in the $Fe_2Mo_3O_8$ material a very narrow many-body excitation forms at the onset of the gap. This is the reason for the first peak

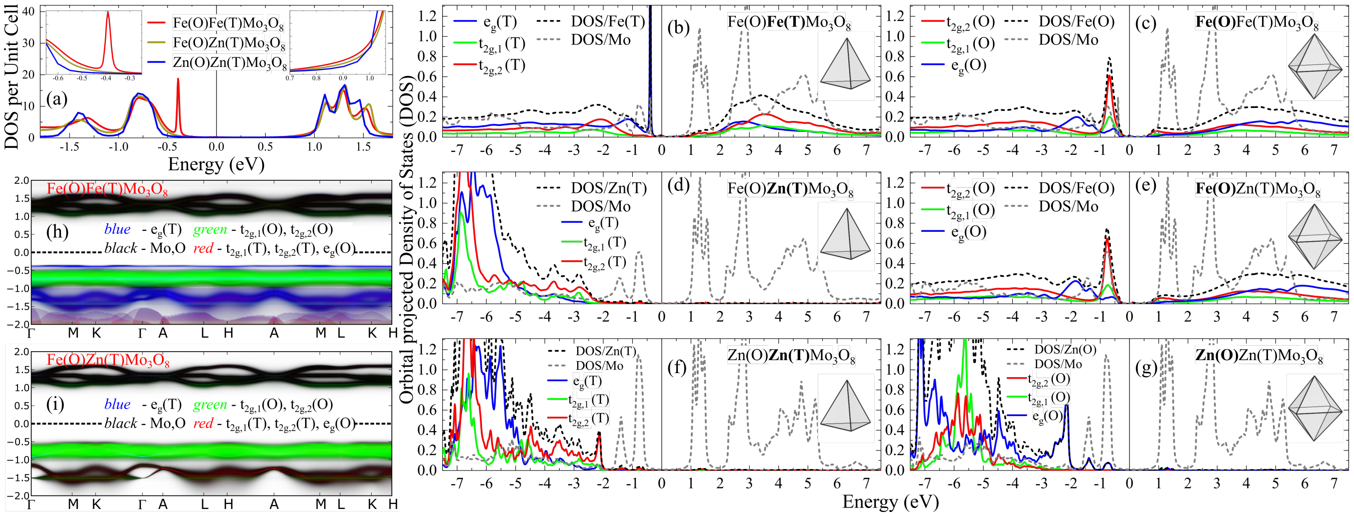

FIG. 2. Density of states (DOS) for A_2Mo$_3$O$_8$ (A = Fe and Zn): (a) total DOS; (b-g) atom and orbital projected DOS; (h, i) schematic view of the orbitals. The (T) and (O) symbols refers to the tetrahedral; and octahedral environments. For example Fe(O) is the label for the Fe ion inside the octahedral environment and e_g(T) is the label for the that orbital for an ion in a tetrahedral environment. The vertical solid lines placed at zero chemical potential. The schematic insets of gray tetrahedra/octahedra are guides to the eye pointing the reader to the electronic states of the transition-metal ions in the corresponding environment. Orbital projected spectral functions for Fe$_2$Mo$_3$O$_8$ in (h) and FeZnMo$_3$O$_8$ in (i).

in the optical conductivity in Fig. 1(h,i).

Figure 2(b-g) displays the density of states (DOS) projected per transition metal center and per orbital in the tetrahedral (T) and octahedral (O) environments. The local point group symmetry is C$_{3v}$. Therefore the e_g states are doubly degenerate, and the t_{2g} states split into a doubly degenerate set ($t_{2g,2}$) and a singly-degenerate state ($t_{2g,1}$). First we notice that Mo states (dotted grey line) are very similar in all compounds. The low-energy excitations are however not on the Mo site when Fe atoms are present. In panel (b), we show that the sharp many-body resonance around -0.4 eV comes primarily from the Fe state in the tetrahedral environment, e_g(T). Panel (c) shows that a broader, but still quite sharp excitations around -0.8 eV comes from the doubly-degenerate $t_{2g,2}$(O) state on the octahedral site. Since both of these rather sharp excitations come from band formation through hybridization, the Mo partial DOS also has a small peak at exactly the same energy. This demonstrates the quasi-particle nature of these peaks, which are Kondo-like peaks that come from screening of the local spin on e_g(T) and $t_{2g,2}$(O) orbitals, although here, the screening is found in an insulator rather than a metal - as expected for many body Kondo peak formation. While broader peaks like that at -0.8 eV are not uncommon in transition-metal compounds and appear for example in monoxides [51, 52], the very narrow resonance appearing in the e_g(T) orbital is unique to Fe$_2$Mo$_3$O$_8$, and is an analog of Zhang-Rice singlet in cuprates [53, 54], because it appears due to screening of the spin 1/2 hole on the Fe-$e_g(T)$ orbitals in the Mott insulating state, with very well defined energy, and strong hybridization mixing with Mo-O trimers.

While Fe$_2$Mo$_3$O$_8$ displays sharp peaks in the valence band spectra in both t_{2g}(O) and e_g(T) orbitals [Fig. 2(b,c)], FeZnMo$_3$O$_8$ has a Zn atom in the tetrahedral site, which is in the d^{10} configuration, and hence inert, with first excitations below -2 eV. The octahedral site containing Fe atoms still shows a sharp valence-band peak in the doubly-degenerate $t_{2g,2}$ orbital, hence this valence band edge peak determines the band gap size in FeZnMo$_3$O$_8$ and is the physical reason for the reduction of the gap as compared to Zn$_2$Mo$_3$O$_8$. Finally, panels (f) and (g) show the Zn-projected DOS in Zn$_2$Mo$_3$O$_8$ in which Zn states are all occupied and far below the Fermi energy, so that the Mo trimer determines the low-energy excitations and the gap size. Because the density of states are momentum-averaged, we also show the spectral functions [Fig. 2(h,i)].

Structure-property relations in the metal-substituted analogs

Figure 3 compares the DOS of the Fe compound with several other transition-metal analogs which have orbital filling between d^5 and d^8 - namely the Mn, Co and Ni analogs. We also display a schematic view of the orbital occupation for both the tetrahedral site (left column) and octahedral site (right column). The gap in each orbital can originate from the band structure due to the periodic potential (band-gap) or from the Mott localization of electrons on a given A site, which we denote as the Mott gap. In principle, we can distinguish between the

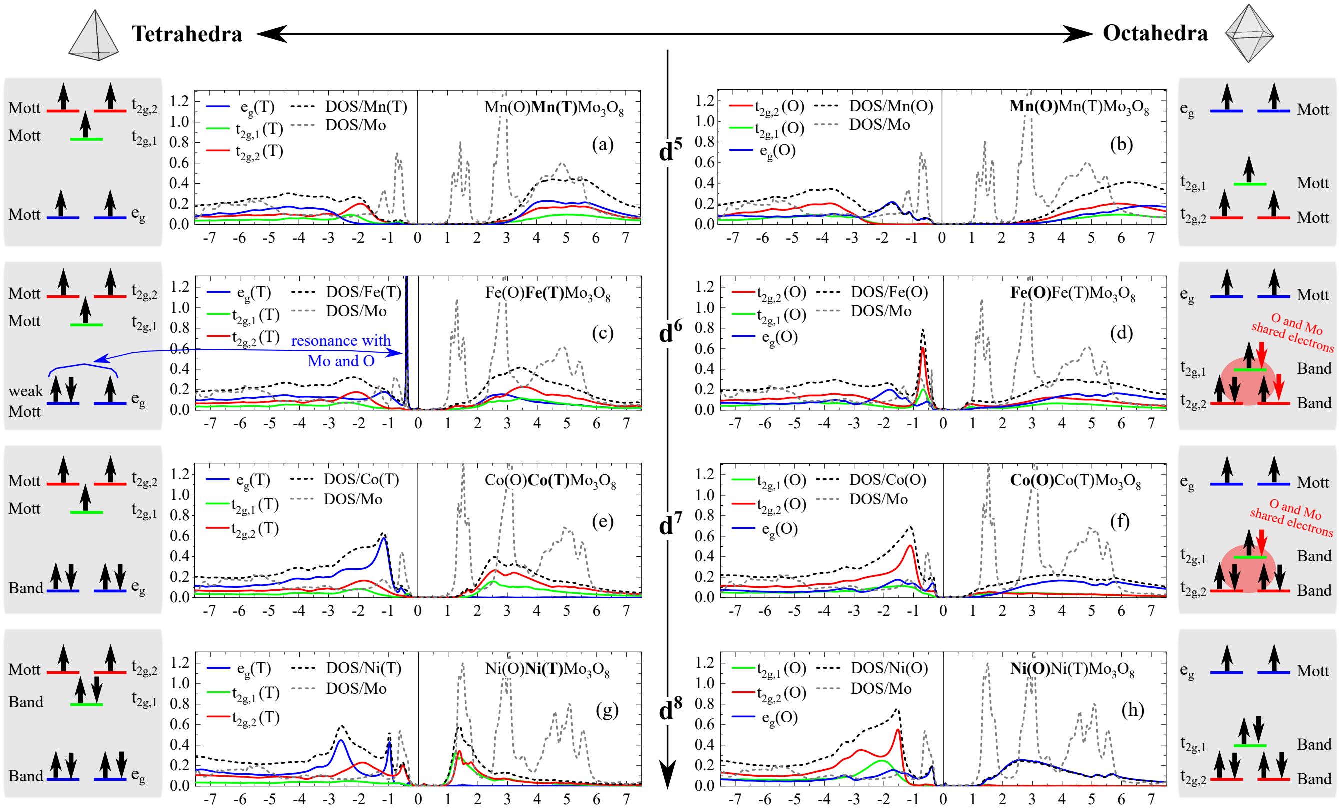

FIG. 3. Atom and orbital projected density of states (DOS) together with a schematic view of the orbital occupation and character for $A_2Mo_3O_8$ (A = Mn, Fe, Co and Zn). Each panel has a schematic view of the electronic orbital occupation (left side) and DOS (right side). Panels (a, c, e, g) refer to the ions inside tetrahedral environments (A(T)), whereas panels (b, d, f, h) refer to ions in octahedral environments (A(O)).

two, because the single-particle spectral function is modified from the DFT bands by self-energy effects, which are either finite (or zero inside the gap) in the case of a band gap, or divergent inside the gap for the case of a Mott gap [55–57]. The latter means that the electron state can no longer be described within the band picture. At the valence edge of the gap, however, the hybridization can still provide an efficient screening channel, even though no itinerant state is present at the Fermi level. In this case a sharp resonance or a quasi-particle multiplet can appear at the gap edge [58] which is temperature dependent and sensitive to small perturbations. We have identified such a many-body resonance in the e_g(T) orbital in $Fe_2Mo_3O_8$ above.

The top panel of Fig. 3 shows calculations for $Mn_2Mo_3O_8$ in which the electrons are in the high-spin d^5 configuration. The Mott gap opens in all orbitals on both tetrahedra and octahedra, which is much larger than the band gap of Mo-trimer. Consequently the band gap and low energy excitations in the Mn and Zn compounds are determined by the same Mo-trimer states and hence are similar. $Fe_2Mo_3O_8$ is the most interesting among all transition metal analogs showing a complex interplay of band gaps, Mott gaps, and quasi-particle multiplets. The t_{2g}(T) states on the tetrahedra are Mott insulating with a large gap. As discussed above, the doubly degenerate e_g(T) orbital contains one hole, which is equally distributed among the two orbitals, and the Mott mechanism opens the gap - even though the self-energy pole is less strong and the gap smaller than in the t_{2g}(T) states. Moreover, at the edge of the gap, strong hybridization, directly computable by the DMFT hybridization function, shows a very strong and narrow peak due to many body effects of screening. With this mechanism, the spin-1/2 of the e_g(T) orbital is screened by the Mo-trimer electrons, a mechanism which is analogous to the Zhang-Rice state in cuprates [53]. Note that this is different from the sharp peak in transition-metal monoxides, called the valence band edge, discussed in Ref. [51, 52]. The latter appears in the antiferromagnetic state, where all gaps are band-like in nature, and the spin states are split by the Zeeman field, hence many-body screening of spin is not possible. Here the spin preserves SU(2) symmetry, and the resonance screens the local spin on Fe.

The octahedral site in the Fe d^6 state contains a combination of Mott gap in the e_g(O) states, and a band gap in the t_{2g}(O) states, a so called orbitally-selective Mott state [36, 37]. Note that the sharp peak at the valence band edge appears as well, even though it is not as sharp as the $e_g(\mathrm{T})$ resonance. Its nature is different, as it appears in band-insulating $t_{2g}(\mathrm{O})$ orbitals, which is similar to the valence band edge discussed in transition metal monoxides [51, 52]. Note that the hybridization and band formation with oxygen and Mo electrons is needed to open the band gap in Fe $t_{2g}(\mathrm{O})$ states, as it contains only four electrons in three nearly degenerate $t_{2g}(\mathrm{O})$ orbitals.

Next we discuss the Co analog, which is in the d^7 configuration. In this case, the $e_g(\mathrm{T})$ orbitals on the tetrahedral site are fully filled, and the $t_{2g}(\mathrm{T})$ orbitals are in the high-spin Mott insulating state with a large gap - larger than Mo-trimer gap. On the octahedral site, the $e_g(\mathrm{O})$ orbitals are Mott-insulating with a large gap, and the $t_{2g}(\mathrm{O})$ states are band-insulating in which Mo and oxygen provide one electron to form a covalent band with the $t_{2g}(\mathrm{O})$ electrons. We note that no sharp low-energy peak is found at the valence band edge, although in principle such a peak is possible.

Figure 3(g,h) displays the Ni analog with its d^8 configuration. In this case, the $e_g(\mathrm{T})$ and the non-degenerate $t_{2g,1}(\mathrm{T})$ orbitals are fully filled, and the doubly-degenerate $t_{2g,2}$ state shows a Mott gap which is comparable to that of the Mo trimer. On the octahedral site, the $t_{2g}(\mathrm{O})$ states are fully filled, and the $e_g(\mathrm{O})$ states are in the half-filled Mott insulating state. This Mott gap is again comparable to the Mo-trimer gap. Hence the reduction of the gap as compared to the Zn analog is minimal.

SUMMARY AND OUTLOOK

To summarize, we measured the optical properties of $Fe_2Mo_3O_8$ and compared our findings with first principles electronic structure calculations. We find a 1.1 eV direct gap composed of heavily mixed charge-transfer excitations that is sensitive to magnetic ordering at 61 K, vibronic coupling that activates on-site d-to-d excitations on the octahedral Fe site, and spin-orbit related excitations riding on top of the tetrahedral Fe site d-to-d excitation below the magnetic ordering temperature. $Fe_2Mo_3O_8$ is a superb platform for unraveling structure-property relationships. What differentiates $Fe_2Mo_3O_8$ from the Zn, Mn, and Ni members of this series is the band-Mott mixing and Zhang-Rice resonance in this d^6 system and how it hybridizes the gap. Taken together, these findings enhance our understanding of charge transfer in quantum cluster magnets and advance the use of this powerful scaffold in new types of charge storage devices.

Research at the University of Tennessee and Rutgers University is supported by the NSF-DMREF program (DMR-1629079 and DMR-1629059). While performing the eDMFT and DFT calculations (at Rutgers, USA), G.L.P was supported by the U.S. Department of Energy, Office of Science, Basic Energy Sciences, as a part of the Computational Materials Science Program, funded by the U.S. Department of Energy, Office of Science, Basic Energy Sciences, Materials Sciences and Engineering Division. While processing theoretical data, analyzing the results and preparing the manuscript (at USV, Romania), G.L.P.'s work was supported by a grant of the Romanian Ministry of Education and Research, CNCS - UEFISCDI, project number PN-III-P1-1.1-TE-2019-1767, within PNCDI III. Access to the x-ray facilities at the Research Complex, Rutherford Appleton Laboratory is gratefully acknowledged.

---

* musfeldt@utk.edu

[1] S. V. Streltsov and D. I. Khomskii, *Orbital physics in transition metal compounds: new trends,* Physics-Uspekhi **60**, 1121 (2017), http://arxiv.org/abs/1711.05409 arXiv:1711.05409.

[2] R. Morrow, R. Mishra, O. D. Restrepo, M. R. Ball, W. Windl, S. Wurmehl, U. Stockert, B. Büchner, and P. M. Woodward, *Independent Ordering of Two Interpenetrating Magnetic Sublattices in the Double Perovskite Sr_2CoOsO_6,* Journal of the American Chemical Society **135**, 18824 (2013).

[3] B. Yan, A. K. Paul, S. Kanungo, M. Reehuis, A. Hoser, D. M. Többens, W. Schnelle, R. C. Williams, T. Lancaster, F. Xiao, J. S. Möller, S. J. Blundell, W. Hayes, C. Felser, and M. Jansen, *Lattice-Site-Specific Spin Dynamics in Double Perovskite Sr_2CoOsO_6,* Physical Review Letters **112**, 147202 (2014), http://arxiv.org/abs/1312.0767 arXiv:1312.0767.

[4] M. Ye, H.-S. Kim, J.-W. Kim, C.-J. Won, K. Haule, D. Vanderbilt, S.-W. Cheong, and G. Blumberg, *Covalency-driven collapse of strong spin-orbit coupling in face-sharing iridium octahedra,* Phys. Rev. B **98**, 201105 (2018).

[5] M. Ye, H.-S. Kim, J.-W. Kim, C.-J. Won, K. Haule, D. Vanderbilt, S.-W. Cheong, and G. Blumberg, *Covalency-driven collapse of strong spin-orbit coupling in face-sharing iridium octahedra,* Phys. Rev. B **98**, 201105(R) (2018).

[6] J. Singleton, J. W. Kim, C. V. Topping, A. Hansen, E.-D. Mun, S. Chikara, I. Lakis, S. Ghannadzadeh, P. Goddard, X. Luo, Y. S. Oh, S.-W. Cheong, and V. S. Zapf, *Magnetic properties of Sr_3NiIrO_6 and Sr_3CoIrO_6: Magnetic hysteresis with coercive fields of up to 55 T,* Phys. Rev. B **94**, 224408 (2016).

[7] K. R. O'Neal, A. Paul, A. Al-Wahish, K. D. Hughey, A. L. Blockmon, X. Luo, S.-W. Cheong, V. S. Zapf, C. V. Topping, J. Singleton, M. Ozerov, T. Birol, and J. L. Musfeldt, *Spin–lattice and electron–phonon coupling in 3d/5d hybrid Sr_3NiIrO_6,* npj Quantum Materials **4**, 48 (2019).

[8] N. D. Khanh, N. Abe, H. Sagayama, A. Nakao, T. Hanashima, R. Kiyanagi, Y. Tokunaga, and T. Arima, *Magnetoelectric coupling in the honeycomb*

antiferromagnet $Co_4Nb_2O_9$, Phys. Rev. B **93**, 075117 (2016).

[9] T. Liang, S. M. Koohpayeh, J. W. Krizan, T. M. McQueen, R. J. Cava, and N. P. Ong, *Heat capacity peak at the quantum critical point of the transverse Ising magnet $CoNb_2O_6$,* Nature Communications **6**, 7611 (2015).

[10] M. O. Yokosuk, H.-S. Kim, K. D. Hughey, J. Kim, A. V. Stier, K. R. O'Neal, J. Yang, S. A. Crooker, K. Haule, S.-W. Cheong, D. Vanderbilt, and J. L. Musfeldt, *Nonreciprocal directional dichroism of a chiral magnet in the visible range,* npj Quantum Materials **5**, 20 (2020).

[11] D. Inosov, *Quantum magnetism in minerals,* Advances in Physics **67**, 149 (2018), http://arxiv.org/abs/1806.10967 arXiv:1806.10967.

[12] J. P. Sheckelton, J. R. Neilson, D. G. Soltan, and T. M. McQueen, *Possible valence-bond condensation in the frustrated cluster magnet $LiZn_2Mo_3O_8$,* Nature Materials **11**, 493 (2012).

[13] M. Mourigal, W. T. Fuhrman, J. P. Sheckelton, A. Wartelle, J. A. Rodriguez-Rivera, D. L. Abernathy, T. M. McQueen, and C. L. Broholm, *Molecular Quantum Magnetism in* $\mathrm{LiZn_2Mo_3O_8}$*,* Phys. Rev. Lett. **112**, 027202 (2014).

[14] Y. Wang, G. L. Pascut, B. Gao, T. A. Tyson, K. Haule, V. Kiryukhin, and S.-W. Cheong, *Unveiling hidden ferrimagnetism and giant magnetoelectricity in polar magnet $Fe_2Mo_3O_8$,* Scientific Reports **5**, 12268 (2015).

[15] T. Kurumaji, S. Ishiwata, and Y. Tokura, *Doping-Tunable Ferrimagnetic Phase with Large Linear Magnetoelectric Effect in a Polar Magnet* $\mathrm{Fe_2Mo_3O_8}$*,* Phys. Rev. X **5**, 031034 (2015).

[16] Y. Li, G. Gao, and K. Yao, *Dzyaloshinskii-Moriya interaction of polar magnet $Fe_2Mo_3O_8$ and its multiferroicity,* EPL (Europhysics Letters) **118**, 37001 (2017).

[17] H. Chen, *Magnetically driven orbital-selective insulator–metal transition in double perovskite oxides,* npj Quantum Materials **3**, 57 (2018), http://arxiv.org/abs/1811.03465 arXiv:1811.03465.

[18] I. V. Solovyev and S. V. Streltsov, *Microscopic toy model for magnetoelectric effect in polar* $\mathrm{Fe_2Mo_3O_8}$*,* Phys. Rev. Materials **3**, 114402 (2019).

[19] S. Nikolaev, I. Solovyev, and S. Streltsov, *Quantum spin liquid and cluster Mott insulator phases in the Mo_3O_8 magnets,* noop arXiv preprint arXiv:2001.07471 (2020).

[20] S. V. Streltsov, D. J. Huang, I. V. Solovyev, and D. I. Khomskii, *Ordering of Fe and Zn Ions and the Magnetic Properties of $FeZnMo_3O_8$,* JETP Letters **109**, 786 (2019), http://arxiv.org/abs/1910.07736 arXiv:1910.07736.

[21] S. Nakayama, R. Nakamura, M. Akaki, D. Akahoshi, and H. Kuwahara, *Ferromagnetic Behavior of $(Fe_{1-y}Zn_y)_2Mo_3O_8$ $(0{\le}y{\le}1)$ Induced by Nonmagnetic Zn Substitution,* Journal of the Physical Society of Japan **80**, 104706 (2011).

[22] W. H. McCarroll, L. Katz, and R. Ward, *Some Ternary Oxides of Tetravalent Molybdenum 1,2,* Journal of the American Chemical Society **79**, 5410 (1957).

[23] G. B. Ansell and L. Katz, *A refinement of the crystal structure of zinc molybdenum(IV) oxide, $Zn_2Mo_3O_8$,* Acta Crystallographica **21**, 482 (1966).

[24] F. Varret, H. Czeskleba, F. Hartmann-Boutron, and P. Imbert, *Étude par effet Mössbauer de l'ion Fe2+ en symétrie trigonale dans les composés du type (Fe, M)$_2Mo_3O_8$ (M = Mg, Zn, Mn, Co, Ni) et propriétés magnétiques de (Fe, Zn)$_2Mo_3O_8$,* Journal de Physique **33**, 549 (1972).

[25] H. Czeskleba, P. Imbert, and F. Varret, *Mössbauer Study of $Fe_2Mo_3O_8$ and $FeZnMo_3O_8$,* AIP Conference Proceedings **5**, 811

[26] T. N. Stanislavchuk, G. L. Pascut, A. P. Litvinchuk, Z. Liu, S. Choi, M. J. Gutmann, B. Gao, K. Haule, V. Kiryukhin, S.-W. Cheong, and A. A. Sirenko, *Spectroscopic and first principle* $\mathrm{DFT}+eDMFT$ *study of complex structural, electronic, and vibrational properties of* $M_2\mathrm{Mo_3O_8}$ *(M =* Fe*, Mn) polar magnets,* Phys. Rev. B **102**, 115139 (2020).

[27] S. Reschke, A. A. Tsirlin, N. Khan, L. Prodan, V. Tsurkan, I. Kézsmárki, and J. Deisenhofer, *Structure, phonons, and orbital degrees of freedom in $Fe_2Mo_3O_8$,* Phys. Rev. B **102**, 094307 (2020).

[28] M. G. Kim, H. Miao, B. Gao, S.-W. Cheong, C. Mazzoli, A. Barbour, W. Hu, S. B. Wilkins, I. K. Robinson, M. P. M. Dean, and V. Kiryukhin, *Imaging antiferromagnetic antiphase domain boundaries using magnetic Bragg diffraction phase contrast,* Nature Communications **9**, 5013 (2018).

[29] S. Yu, B. Gao, J. W. Kim, S.-W. Cheong, M. K. L. Man, J. Madéo, K. M. Dani, and D. Talbayev, *High-Temperature Terahertz Optical Diode Effect without Magnetic Order in Polar* $\mathrm{FeZnMo_3O_8}$*,* Phys. Rev. Lett. **120**, 037601 (2018).

[30] B. Csizi, S. Reschke, A. Strinic, L. Prodan, V. Tsurkan, I. Kézsmárki, and J. Deisenhofer, *Magnetic and vibronic THz excitations in multiferroic $Fe_{1.8}Zn_{0.2}Mo_3O_8$,* noop arXiv preprint arXiv:2004.02443 (2020).

[31] Y. M. Sheu, Y. M. Chang, C. P. Chang, Y. H. Li, K. R. Babu, G. Y. Guo, T. Kurumaji, and Y. Tokura, *Picosecond Creation of Switchable Optomagnets from a Polar Antiferromagnet with Giant Photoinduced Kerr Rotations,* Phys. Rev. X **9**, 031038 (2019).

[32] A. Biswas, H. Triki, Q. Zhou, S. P. Moshokoa, M. Z. Ullah, and M. Belic, *Cubic–quartic optical solitons in Kerr and power law media,* Optik **144**, 357 (2017).

[33] Q. Chen, A. Verrier, D. Ziat, A. J. Clune, R. Rouane, X. Bazier-Matte, G. Wang, S. Calder, K. M. Taddei, C. R. dela. Cruz, A. I. Kolesnikov, J. Ma, J.-G. Cheng, Z. Liu, J. A. Quilliam, J. L. Musfeldt, H. D. Zhou, and A. A. Aczel, *Realization of the orbital-selective Mott state at the molecular level in* $\mathrm{Ba_3LaRu_2O_9}$*,* Phys. Rev. Materials **4**, 064409 (2020).

[34] G. L. Pascut and K. Haule, *Role of orbital selectivity on crystal structures and electronic states in $BiMnO_3$ and $LaMnO_3$ perovskites,* noop arXiv preprint arXiv:2005.12179 (2020), http://arxiv.org/abs/2005.12179 arXiv:2005.12179 [cond-mat.str-el].

[35] A. I. Lichtenstein, M. I. Katsnelson, and G. Kotliar, *Finite-Temperature Magnetism of Transition Metals: An ab initio Dynamical Mean-Field Theory,* Phys. Rev. Lett. **87**, 067205 (2001).

[36] V. Anisimov, I. Nekrasov, D. Kondakov, T. Rice, and M. Sigrist, *Orbital-selective Mott-insulator transition in $Ca_{2-x}Sr_xRuO_4$,* The European Physical Journal B **25**, 191 (2002).

[37] L. de'Medici, A. Georges, and S. Biermann, *Orbital-selective Mott transition in multiband systems: Slave-spin representation and dynamical mean-field theory,*

Phys. Rev. B **72**, 205124 (2005).

[38] K. Haule and G. L. Pascut, *Mott Transition and Magnetism in Rare Earth Nickelates and its Fingerprint on the X-ray Scattering,* Scientific Reports **7**, 10375 (2017), http://arxiv.org/abs/1703.08196 arXiv:1703.08196.

[39] P. Blaha, K. Schwarz, G. Madsen, D. Kvasnicka, J. Luitz, R. Laskowsk, F. Tran, L. Marks, and L. Marks, noop *WIEN2k: An Augmented Plane Wave Plus Local Orbitals Program for Calculating Crystal Properties* (Techn. Universitat, 2019).

[40] K. Haule, noop *DMFT code* (2007-2020), `http://hauleweb.rutgers.edu/tutorials/`.

[41] K. Haule, *Structural predictions for Correlated Electron Materials Using the Functional Dynamical Mean Field Theory Approach,* Journal of the Physical Society of Japan **87**, 041005 (2018).

[42] K. Haule, C.-H. Yee, and K. Kim, *Dynamical mean-field theory within the full-potential methods: Electronic structure of* $CeIrIn_5$*,* $CeCoIn_5$*, and* $CeRhIn_5$*,* Phys. Rev. B **81**, 195107 (2010).

[43] A. Paul and T. Birol, *Applications of DFT + DMFT in Materials Science,* Annual Review of Materials Research **49**, 31 (2019), http://arxiv.org/abs/https://doi.org/10.1146/annurev-matsci-070218-121825 https://doi.org/10.1146/annurev-matsci-070218-121825.

[44] K. Haule and G. L. Pascut, *Forces for structural optimizations in correlated materials within a DFT+embedded DMFT functional approach,* Phys. Rev. B **94**, 195146 (2016).

[45] J. P. Perdew, K. Burke, and M. Ernzerhof, *Generalized Gradient Approximation Made Simple,* Phys. Rev. Lett. **77**, 3865 (1996).

[46] K. Haule, *Exact Double Counting in Combining the Dynamical Mean Field Theory and the Density Functional Theory,* Phys. Rev. Lett. **115**, 196403 (2015).

[47] K. Haule, *Quantum Monte Carlo impurity solver for cluster dynamical mean-field theory and electronic structure calculations with adjustable cluster base,* Phys. Rev. B **75**, 155113 (2007).

[48] J. I. Pankove, noop *Optical Processes in Semiconductors* (Dover Publications; 2nd Revised ed. edition, 2010) p. 448.

[49] P. K. Sarswat and M. L. Free, *A study of energy band gap versus temperature for* Cu_2ZnSnS_4 *thin films,* Physica B: Condensed Matter **407**, 108 (2012).

[50] K. P. O'Donnell and X. Chen, *Temperature dependence of semiconductor band gaps,* Applied Physics Letters **58**, 2924 (1991).

[51] S. Mandal, K. Haule, K. M. Rabe, and D. Vanderbilt, *Systematic beyond-DFT study of binary transition metal oxides,* npj Computational Materials **5**, 115 (2019), http://arxiv.org/abs/1907.10498 arXiv:1907.10498.

[52] S. Mandal, K. Haule, K. M. Rabe, and D. Vanderbilt, *Influence of magnetic ordering on the spectral properties of binary transition metal oxides,* Phys. Rev. B **100**, 245109 (2019).

[53] F. C. Zhang and T. M. Rice, *Effective Hamiltonian for the superconducting Cu oxides,* Phys. Rev. B **37**, 3759 (1988).

[54] H. Eskes and G. A. Sawatzky, *Tendency towards Local Spin Compensation of Holes in the High-*T_c *Copper Compounds,* Phys. Rev. Lett. **61**, 1415 (1988).

[55] E. Pavarini, E. Koch, R. Scalettar, and R. Martin, eds., *The Physics of Correlated Insulators, Metals, and Superconductors*, Schriften des Forschungszentrums Jülich Reihe Modeling and Simulation, Vol. 7 (Forschungszentrum Jülich GmbH Zentralbibliothek, Verlag, Jülich, 2017) p. 450 p.

[56] D. O. Demchenko, A. V. Joura, and J. K. Freericks, *Effect of Particle-Hole Asymmetry on the Mott-Hubbard Metal-Insulator Transition,* Phys. Rev. Lett. **92**, 216401 (2004).

[57] G. Kotliar, S. Y. Savrasov, K. Haule, V. S. Oudovenko, O. Parcollet, and C. A. Marianetti, *Electronic structure calculations with dynamical mean-field theory,* Rev. Mod. Phys. **78**, 865 (2006).

[58] C.-H. Yee, G. Kotliar, and K. Haule, *Valence fluctuations and quasiparticle multiplets in plutonium chalcogenides and pnictides,* Phys. Rev. B **81**, 035105 (2010) .